# Simulation of 3D interlock composite preforming

E. De Luycker [a,b], F. Morestin [a], P. Boisse [a,*], D. Marsal [b]

[a] Université de Lyon, INSA-Lyon, LaMCoS CNRS UMR 5259, 7 avenue Jean Capelle, F-69621 Villeurbanne, France
[b] Snecma Villaroche W/YQMM, F-77550, France

*Keywords:*
Fabrics
Textiles
Finite element analysis
Forming
Preform
Interlock Fabrics

A B S T R A C T

The ply to ply interlock fabric preform enables to manufacture, by R.T.M. process, thick composite parts that are resistant to delamination and cracking. Numerical simulation of interlock reinforcement forming allows to determine conditions for feasibility of the process and above all to know the position of fibres in the final composite part. For this forming simulation, specific hexahedral finite elements made of segment yarns are proposed. Position of each yarn segment within the element is taken into account. This avoids determination of a homogenized equivalent continuous law that would be very difficult considering the complexity of the weaving. Transverse properties of fabric are taken into account within a hypoelastic constitutive law. A set of 3D interlock fabric forming simulations shows the efficiency of the proposed approach.

## 1. Introduction

### *1.1. Layer interlock weaves*

Laminated composites with 2D layered reinforcements have been used with outstanding success for several decades in aircraft [1,2], high performance automotive [3] maritime craft [4] and civil engineering [5,6]. Nevertheless the use of these laminated composites is restricted by manufacturing problems and some inferior mechanical properties. When the thickness of a composite part is large, the high labour requirement in manual lay up of plies can be expensive. In addition, achievement of complex shapes often needs to build them from several laminated parts that must be joined. Application of 2D laminated composites has been restricted by their low resistance to delamination cracking due to their poor interlaminar fracture toughness. This possible brittle fracture is unacceptable in some critical parts, especially in aerospace applications. In order to overcome these difficulties, composites with 3D fibre architecture have been proposed. Among these 3D fibre architectures, the ply to ply interlock fabric is one of the most interesting [7–10]. The basic architecture of an interlock fabric is shown in Fig. 1. Two layers of weft yarns are joined by the weaving of the warp yarns. Consequently, all the yarns through the thickness are joined by the weaving. The resulting material is 3D with no third yarn set in the transverse direction but the properties through the thickness are much improved. Above all, the possible delaminations of the 2D laminated composites are overcome.

* Corresponding author. Tel.: +33 4 72 43 63 96; fax: +33 4 72 43 85 25.
*E-mail address:* Philippe.Boisse@insa-lyon.fr (P. Boisse).

If Fig. 1 shows the basic architecture of layer interlock weaves, the recent advances in the field of computer controlled Jacquard looms allow to obtain much more complicated interlock weavings. The path of warp yarns around weft yarns can be non-periodic; the sections of the yarns can be different in various places of the reinforcement. Finally the number of weft yarns can vary along the part. The resulting preform is a complex 3D assembly of yarns such as shown in the example diagram Fig. 2. These complex architectures of interlock fabrics have great benefits. First thickness of the preform can be large (up to 100 mm) (Example in Fig. 3). Above all, design of the weaving can be optimized in order to obtain optimal mechanical properties. The architecture of the weaving can be changed to reduce damage in a critical area of the structure. These advantages added to the fact that interlock fabrics are damage tolerant due to the resistance offered by interlacing tows to crack propagation, lead to use this technology for some aeronautical applications such as aero engine fan blades (see Fig. 4).

### *1.2. R.T.M. Process. Objective of the current work*

From the interlock fabric preform, composite parts are obtained by R.T.M. process (Resin Transfer Moulding) [11–13]. This process is composed of two main stages (Fig. 5). First, the interlock fabric is formed in order to obtain the geometry of the final part that can be complex (for instance in Fig. 4). In particular when this geometry is double curved, shear strains are necessary to reach the shape. Analysis and simulation of this preforming stage in case of the interlock 3D reinforcements is the purpose of this present paper. Subsequently, resin (usually thermoset) is injected within porous fibrous reinforcement. The composite structure obtained is this way can be thick, without layer stacking and with complex shapes.

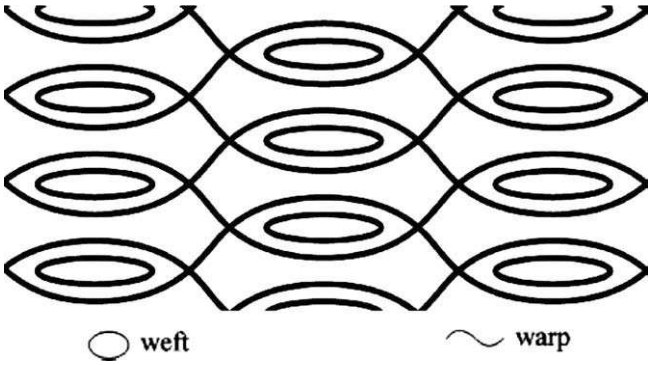


**Fig. 1.** Basic architecture of an interlock fabric.

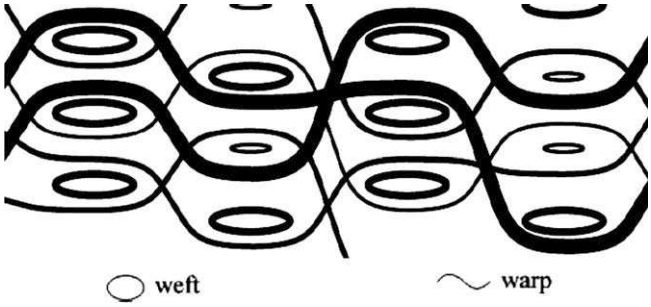


**Fig. 2.** Example of complex layer interlock weave.

**Fig. 3.** Large thickness preform.

They have improved mechanical properties especially resistance to crack propagation. Furthermore the finishing is good.

Preforming stage has important consequences on the following. First it conditions injection stage. Strains change the permeability of the interlock fabric. Shear strains tend to "close" channels of the flow and compression of the reinforcement in the mould are necessary to avoid flows between the fabric and the tools and to set prescribed thickness of the part. Above all, preforming stage determines the position of yarns in the final composite part. This position and especially direction of fibers plays a predominant role in the mechanical properties of the composite structure. It must be taken very accurately into account in structural analyses (rigidity, damage, fracture, vibrations....) that must be performed on the composite part especially if it is a critical structure. Thus simulation of the preforming stage has two main goals:

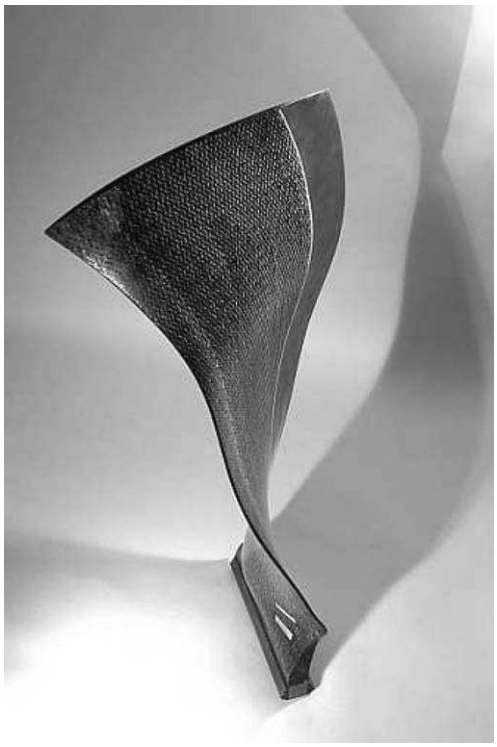

**Fig. 4.** Plane motor blade (Courtesy of Snecma, Groupe Safran).

– Determine if the preforming process is possible or what are the manufacturing conditions that make it possible. In particular, strains of the reinforcement must not exceed some limits. Angle variations between warp and weft yarns are limited (30–50° depending on the reinforcement). Tensile strain of yarns must remain very small. All strains and especially compressive strain must insure that there is no local or global buckling.
– Provide fiber directions and densities after the preforming in order to be able to simulate resin injection and structural behaviour of the final composite part.

The objective of this present paper is to propose a simulation method for 3D interlock fabric forming. The different methods proposed for draping simulations of thin fabrics (2D) [14–18] cannot be used in this 3D problem. The proposed simulation method is based on a specific hexahedral finite element that is composed of yarns segments. Position of each yarn is taken into account in accordance with the geometry obtained after the weaving process. Tensile rigidities of yarns lead to the main part of the element stiffness. Beside this stiffness, the other rigidities of the interlock preform due to transverse properties of the yarns and frictions are second-order. Nevertheless they can be important especially in the direction where a deformation can occur without yarn stretching. These rigidities are supposed to be those of an isotropic hypoelastic material. A set of elementary tests (bias test and picture frame test) and of forming processes shows the efficiency of the proposed approach.

### *1.3. Notations*

Tensors are denoted by underlined letter ($\underline{X}$ is a first order tensor, $\underline{\underline{X}}$ is a second-order tensor...). Matrices of components in the basic frame are denoted by a bold letter $\mathbf{X}$. When necessary, the basis is specified as $[\mathbf{X}]_{ei}$. Time derivative of X is denoted $\dot{X} = \frac{dX}{dt}$ and $\ddot{X} = \frac{d^2X}{dt^2}$.

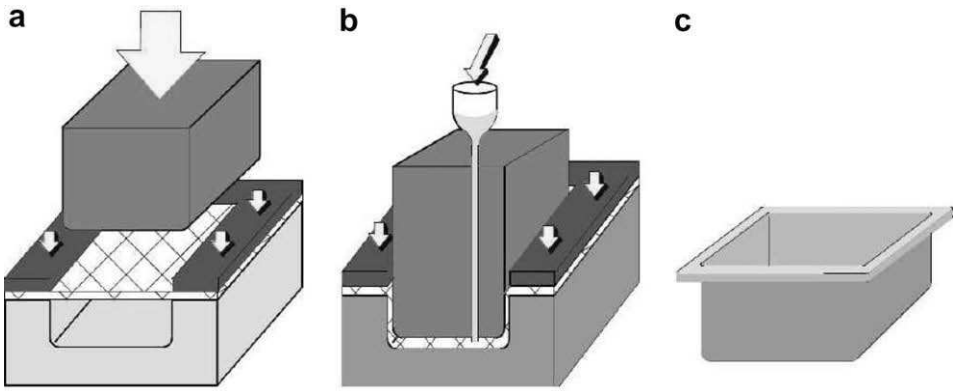


**Fig. 5.** The two main steps of R.T.M process (a) forming of the fibrous part; (b) resin injection and polymerisation and (c) final composite part.

## 2. Interlock fabrics preforming simulation

### *2.1. The problem to solve and the different possible approaches*

The interlock fabrics under consideration are those presented in Fig. 2. The preform is thick and the mechanical problem is 3D. The position of yarns is arbitrary and generally there is no periodicity. On the other hand, position of each yarn is known and can be precisely given after the weaving process.

As for all textile reinforcement forming simulation, the multiscale nature of the reinforcement allows us to consider a continuous or a discrete approach for the simulation [19]. The textile reinforcement is not strictly continuous because some sliding occurs between fibres and yarns when the fabric is strained. Nevertheless, a continuous material superimposed on the fibrous material can be postulated. Such approaches are numerous for the composite reinforcement [15–17,20–22]. If these models can easily be implemented in standard finite elements, identification of the homogenized material parameters remains a difficult and open problem because finite strains and fiber orientations update must be taken into account. Furthermore, in the present case of complex interlock fabrics (Fig. 2), there is no periodicity and the homogenized material should be determined at each point of the reinforcement.

The opposite approach is to see the fibrous reinforcement as a set of elements at lower scales, such as the yarns, woven cells, fibers, etc. The FE analysis is then concerned with those elements that are in contact or are linked by springs [23–30]. The advantage over the continuous approach is that description of internal structure of the reinforcement naturally accounts for some aspects of the material, such as directions of fibers and contact between fibers. Nevertheless, it is difficult to define models that are efficient enough at mesoscale but simple enough to be able to analyze a forming process. In the case of 3D interlock weave preforming simulations, a discrete approach would need finite element modeling of each yarn. The kinematics of each tow should describe the transverse section crushing. Furthermore the contact with all neighbouring yarns should be taken into account. Considering the number of yarns in a preform, such a finite element analysis can be hardly foreseen today within large deformations. (There may be 10 thousands of yarns in a complex preform).

The proposed approach that is described below is a compromise between continuous and discrete approaches [18,19]. It associates a 3D finite element approximation to a discrete description of yarns within the element. It uses exact initial position of yarns within the preform that is known after the weaving, does not need a homogenized mechanical behaviour and requires a reasonable number of 3D finite elements from a computational point of view.

### *2.2. Specific dynamic equation. Explicit scheme*

Mechanical behaviour of the structure realized with layer interlock weaves is very specific. Stiffness of a yarn made of a very large number of small continuous fibres (usually 3 K to 48 K fibres) is mainly a tensile rigidity in the direction tangent to the yarn. Accounting for the very small fibre diameter (5 μm to 20 μm for carbon aramid or glass fibres) and for possible relative motions between fibres and yarns, bending stiffness, but also transverse compression and shear rigidities are small in comparison to tensile stiffness. Deformation of the interlock fabric during the preforming process is mainly led by yarns under tension. The other rigidities and corresponding strain energies only play a second-order role. This must be nevertheless moderated because in some directions, stiffness due to yarn tensions can be negligible and in this case other rigidities play a major role.

Within the virtual work principle, the internal virtual work of tension $W^t_{\text{int}}$ and the other internal virtual works $W^o_{\text{int}}$ are distinguished:

$$W^t_{\text{int}}(\underline{\eta}) + W^o_{\text{int}}(\underline{\eta}) - W_{\text{ext}}(\underline{\eta}) = -W_{\text{acc}}(\underline{\eta}) \tag{1}$$

$\forall \underline{\eta}$ a virtual displacement field such as $\underline{\eta} = 0$ on the boundary with prescribed displacements. $W_{\text{ext}}$ and $W_{\text{acc}}$ are the virtual works due to exterior loads and acceleration quantities. Because the forming is mainly led by yarns in tension accounting for their rigidities that are much larger than others, the modelling effort will mainly concern the tension part $W^t_{\text{int}}$. In this term the complete geometry of each yarn will be taken into account. The second-order term $W^o_{\text{int}}$ may be described in a more simple way. In the present work, a simple form will be considered for this part in order to render identifications of material data simpler and because complexity of the interlock preform is included in the tension term.

Although most forming process are quasi-static, majority of codes (and especially commercial ones) for material forming simulations are based on explicit dynamic approaches [19,32,33] that have proved to be numerically more efficient than implicit ones. This explicit approach will be used in the present work. It will be checked that dynamic effects are small enough not to modify results of simulation.

Within a finite element approximation, the dynamic Eq. (1) written in the set of degrees of freedom leads to:

$$\mathbf{M}\ddot{\mathbf{u}}_n = \mathbf{F}_{\text{ext}} - \mathbf{F}_{\text{int}} \tag{2}$$

$$\text{with} \quad W_{\text{acc}}(\underline{\eta}) = \boldsymbol{\eta}_n^T \mathbf{M}\ddot{\mathbf{u}}_n \quad W_{\text{ext}}(\underline{\eta}) = \boldsymbol{\eta}_n^T \mathbf{F}_{\text{ext}} \tag{3}$$

$$W^t_{\text{int}}(\underline{\eta}) + W^0_{\text{int}}(\underline{\eta}) = \boldsymbol{\eta}_n^T \mathbf{F}_{\text{int}} = \boldsymbol{\eta}_n^T (\mathbf{F}^t_{\text{int}} + \mathbf{F}^o_{\text{int}}) \tag{4}$$

$\mathbf{u}_n$ and $\boldsymbol{\eta}_n$ are single column matrix of nodal displacement and virtual displacement components. $\mathbf{M}$ is the mass matrix, $\mathbf{F}_{\text{ext}}$ and $\mathbf{F}_{\text{int}}$

are single column matrix of components of the exterior and interior nodal loads. $\mathbf{F}_{\text{ext}}$ is given by the exterior loads on the structure.

On a time step $\Delta t^i$, from $t^i$ to $t^{i+1}$, the central difference scheme gets the solution $\mathbf{u}_n^{i+1}$ from $u_n^i$ by:

$$\mathbf{u}_n^{i+1} = \mathbf{u}_n^i + \dot{\mathbf{u}}_n^{i+1/2}\Delta t^i \tag{5}$$

$$\dot{\mathbf{u}}_n^{i+1/2} = \dot{\mathbf{u}}_n^{i-1/2} + \frac{1}{2}(\Delta t^{i-1} + \Delta t^i)\ddot{\mathbf{u}}_n^i \tag{6}$$

$$\ddot{\mathbf{u}}_n^i = \mathbf{M}_D^{-1}(\mathbf{F}_{\text{ext}}^i - \mathbf{F}_{\text{int}}^i) \tag{7}$$

$\mathbf{M}_D$ is the lumped mass matrix [34]. The time step size has to ensure stability condition of the integration scheme, accounting for element size and material data [31].

Definition of the specific finite element for interlock fabric forming will consist in giving expression of the interior loads vectors due to tension stiffnesses $\mathbf{F}_{\text{int}}^t$ and to other rigidities $\mathbf{F}_{\text{int}}^o$ in order to apply the explicit scheme (5)–(7).

## 3. Specific hexahedral finite element

### 3.1. Nodal loads due to tensions in yarns

#### 3.1.1. Finite element containing fibrous yarns

The 3D interlock woven preform is meshed in a set of 3D finite elements such as the one shown in Fig. 6. Yarn segments are crossing the hexahedral element. The interpolation functions of the element are the classical tri-linear functions of the height node hexahedral finite element. In order to be consistent with this interpolation, the yarn segments are straight. This assumption and its consequences will be discussed below (Section 3.1.3). The finite element is Lagrangian (as it is standard in solid mechanics). Material in an element is constant during the deformation and positions of yarn in the reference frame of the element (i.e. in the material frame) are constant. Knowledge of these positions is an important data of the problem and influence stiffness and damage properties [35]. After the weaving, the position of each yarn in the preform is known and consequently determines the position of yarn segments in the element when the preform is meshed in 3D finite elements. In practice, the weaver can provide a record of yarn position that it needs for the weaving process.

#### 3.1.2. Tensile nodal loads

$\underline{h}_1^p$ is the unit vector in the direction of the number $p$ yarn. The tension vector in the yarn $p$ is defined as follows:

$$\underline{T}^p = \int_{S^p} \sigma_{11}^p \mathrm{d}S \underline{h}_1^p \tag{8}$$

where $\sigma_{11}^p = \underline{h}_1^p.(\underline{\underline{\sigma}}^p \cdot \underline{h}_1^p)$ is the axial component of the Cauchy stress in the direction of the yarn $p$ and $S^p$ is the section of the yarn $p$. The virtual internal work due to tension of the yarn segment $p$ is:

$$W_{\text{int}}^{\text{tp}}(\underline{\eta}) = \int_{L^p} T^p \varepsilon^p(\underline{\eta})\mathrm{d}L \tag{9}$$

$L^p$ is the length of the yarn segment number $p$ and $\varepsilon^p(\underline{\eta}) = \underline{h}_1^p.(\underline{\underline{\nabla}}^S(\underline{\eta}).\underline{h}_1^p)$ is the component of the symmetrical gradient of the virtual displacement $\underline{\eta}$ in the direction of the yarn. For the number $e$ element:

$$W_{\text{int}}^{\text{te}}(\underline{\eta}) = \sum_{p=1}^{nye} \int_{L^p} T^p \varepsilon^p(\underline{\eta})\mathrm{d}L = \boldsymbol{\eta}_n^{eT}\mathbf{F}_{\text{int}}^{\text{te}} \tag{10}$$

where $nye$ is the number of yarn segments in the element $e$ and $\mathbf{F}_{\text{int}}^{\text{te}}$ is the single column matrix of elementary tensile nodal loads.

The global tensile nodal loads $\mathbf{F}_{\text{int}}^t$ of Eq. (4) is the assembly of $\mathbf{F}_{\text{int}}^{\text{te}}$ on all elements.

The virtual strain $\varepsilon^p(\underline{\eta})$ will now be expressed as a function of nodal virtual displacements in order to determine $\mathbf{F}_{\text{int}}^{\text{te}}$. Derivatives of the position $\underline{x}$ of a point within the finite element relatively to natural coordinates in the reference element $(\xi^1, \xi^2, \xi^3) \in [-1, 1]^3$ or material coordinates define the covariant material vectors:

$$\underline{g}_i = \frac{\partial \underline{x}}{\partial \xi_i} \quad i = 1 \text{ to } 3 \tag{11}$$

The corresponding contravariant vectors $\underline{g}^i$ are such as $\underline{g}^i \cdot \underline{g}_j = \delta_j^i$. The vector $\underline{h}_1^p$ is known for each yarn segment $p$ and its components in the frame defined by the covariant vector $\underline{g}_i$ are denoted $\alpha_i^p$:

$$\underline{h}_1^p = \sum_{i=1}^{3} \alpha_i^p \underline{g}_i \quad \alpha_i^p = \underline{h}_1^p \cdot \underline{g}^i \tag{12}$$

The interpolation functions of the eight node hexahedral element are the standard tri-linear functions:

$$N^k(\xi^1, \xi^2, \xi^3) = \frac{1}{8}(1 \pm \xi^1)(1 \pm \xi^2)(1 \pm \xi^3) \tag{13}$$

The element is isoparametric: displacement and position of a point $M$ within the element are interpolated in function of nodal quantities:

$$\underline{u}(M) = \sum_{k=1}^{8} N^k(\xi^1, \xi^2, \xi^3)\underline{u}^k \qquad \mathbf{u}(M) = \mathbf{N}\mathbf{u}_n^e \tag{14}$$

$$\underline{x}(M) = \sum_{k=1}^{8} N^k(\xi^1, \xi^2, \xi^3)\underline{x}^k \qquad \mathbf{x}(M) = \mathbf{N}\mathbf{x}_n^e \tag{15}$$

The covariant vectors $\underline{g}_i$ depend on nodal positions:

$$\underline{g}_i = \sum_{k=1}^{8} \frac{\partial N^k}{\partial \xi_i}\underline{\mathbf{x}}^k \text{ in a matrix form } \mathbf{g}_i = \mathbf{G}_i\mathbf{x}_n^e \tag{16}$$

The components of the symmetrical displacement gradient are function of the covariant vectors:

$$\underline{\underline{\nabla}}^S(\underline{\eta}) = \frac{1}{2}\left(\frac{\partial \underline{\eta}}{\partial \xi_j} \cdot \underline{g}_i + \frac{\partial \underline{\eta}}{\partial \xi_i} \cdot \underline{g}_j\right)\underline{g}^i \otimes \underline{g}^j = \bar{\varepsilon}_{ij}(\underline{\eta})\underline{g}^i \otimes \underline{g}^j \tag{17}$$

$$\text{i.e. } \bar{\varepsilon}_{ij}(\underline{\eta}) = \mathbf{B}_{ij}\boldsymbol{\eta}_n^e \tag{18}$$

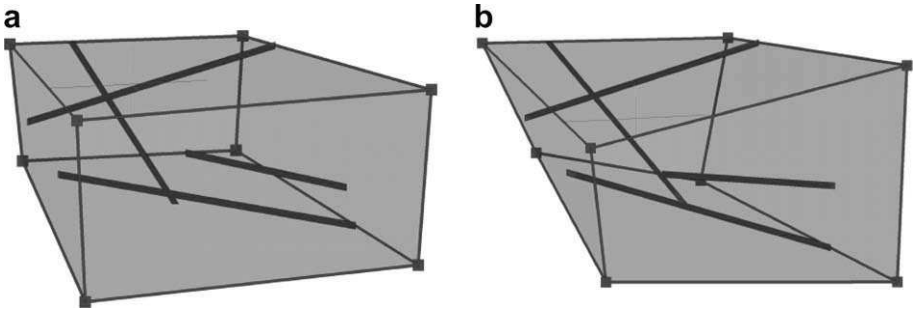


**Fig. 6.** Height node hexahedral finite element containing fibrous yarns (a) Initial and (b) Deformed.

where the single line $\mathbf{B}_{ij}$ matrix is:

$$\mathbf{B}_{ij} = \frac{1}{2}\mathbf{x}_n^{eT}\left(\mathbf{G}_j^T\mathbf{G}_i + \mathbf{G}_i^T\mathbf{G}_j\right) \tag{19}$$

For the yarn segment number $p$, the virtual strain in the yarn direction $\underline{h}_1^p$ is:

$$\varepsilon^p(\underline{\eta}) = \underline{h}_1^p.\left(\underline{\underline{\nabla}}^S(\underline{\eta}) \cdot \underline{h}_1^p\right) = \bar{\varepsilon}_{ij}(\underline{\eta})\left(\underline{g}^i \cdot \underline{h}_1^p\right)\left(\underline{g}^j \cdot \underline{h}_1^p\right) \tag{20}$$

$$\varepsilon^p(\underline{\eta}) = \alpha_i^p\alpha_j^p\mathbf{B}_{ij}\boldsymbol{\eta}_n^e \tag{21}$$

The elementary tensile nodal load is given by:

$$\mathbf{F}_{\text{int}}^{\text{te}} = \sum_{p=1}^{nye}\int_{L^p} T^p\alpha_i^p\alpha_j^p\mathbf{B}_{ij}^T\mathrm{d}L \tag{22}$$

and eventually, taking the into account Eq. (19),

$$\begin{aligned}\alpha_i^p\alpha_j^p\mathbf{B}_{ij} &= \tfrac{1}{2}\left(\left(\alpha_i^p\alpha_j^p\mathbf{x}_n^{eT}\mathbf{G}_j^T\right)\mathbf{G}_i + \left(\alpha_i^p\alpha_j^p\mathbf{x}_n^{eT}\mathbf{G}_i^T\right)\mathbf{G}_j\right)\\ &= \left(\alpha_i^p\mathbf{x}_n^{eT}\mathbf{G}_i^T\right)\left(\alpha_j^p\mathbf{G}_j\right) = \mathbf{h}^{pT}\left(\alpha_j^p\mathbf{G}_j\right)\end{aligned} \tag{23}$$

and Eq. (22) becomes,

$$\mathbf{F}_{\text{int}}^{\text{te}} = \sum_{p=1}^{nye}\int_{L^p} T^p\alpha_i^p\mathbf{G}_i^T\mathbf{h}^p\mathrm{d}L \tag{24}$$

*3.1.3. Yarn tension update*

The explicit scheme (5)–(7) gives nodal displacement and velocity fields at time $t^{i+1}$. The value of the tension in the yarn $T^{p\ i+1}$ at time $t^{i+1}$ must be computed, in particular in order to preform the next time step. In each yarn segment of the element e:

$$T^{p\,i+1} = T^{p\,i} + \Delta T^p \tag{25}$$

with

$$\Delta T^p = C^{p\,i}\frac{L^{p\,i+1} - L^{p\,i}}{L^{p\,i}} \tag{26}$$

$C^p$ is the tensile stiffness of the yarn. If $C^p$ is constant during the preforming, then:

$$T^{p\,i+1} = C^p\int_0^{t^{i+1}}\frac{\mathrm{d}L}{L} = C^p\mathrm{Log}\frac{L^{p\,i+1}}{L_0^p} \tag{27}$$

In this case, the tensile law relates tension to the logarithmic strain in the yarn direction.

*3.2. Nodal loads due to other rigidities*

*3.2.1. Rate constitutive equations*

Main part of mechanical behaviour of the interlock preform during the forming process is due to tensile stiffness of yarns. Nevertheless other aspects such as transverse compression rigidity of yarns, friction between yarns and fibres add some stiffness to the preform. These rigidities are second-order in comparison with tensile rigidities of yarns; still, they can be important, especially in the directions in which tensile stiffness of yarns does not generate a rigidity of the preform. In particular, that is the case for global transverse compression of the preform and some shear strains. Geometrical and physical descriptions of yarns, fibres, interfaces concerned in these rigidities are very complex. Since it is about second-order rigidities, their modelling has to be simple. Complexity of the preform has been taken into account in the principal part of rigidity due to tensile stiffness of yarns. Consequently it is assumed that second rate rigidities can be modelled by those of an isotropic hypoelastic material. These constitutive models (also called rate constitutive equations) are widely used in F.E. codes to model isotropic mechanical behaviour of continuous material at large strain [32,33,37,38]. They can conveniently be extended to plasticity [33,39,40] (This point will be briefly discussed in Section 3.2.2).

An objective derivative of Cauchy stress $\underline{\underline{\boldsymbol{\sigma}}}^{o\nabla}$ is calculated from the strain rate $\underline{\underline{\mathbf{D}}}$:

$$\underline{\underline{\sigma}}^{o\nabla} = \underline{\underline{C}}^o : \underline{\underline{D}} \tag{28}$$

In the same way as in Eqs. (1) and (4), the superscript $o$ refers to properties of the preform that are complementary to those due to yarn tensile properties. $\underline{\underline{\mathbf{C}}}^o$ is an isotropic elastic tensor. Objective derivative is a derivative for an observer who is fixed in the rotated frame that is following as much as possible material during deformation. In the present work objective derivative is Jaumann's one [41]:

$$\underline{\underline{\sigma}}^{o\nabla} = \underline{\underline{Q}}.\left(\frac{\mathrm{d}}{\mathrm{d}t}\left(\underline{\underline{Q}}^T.\underline{\underline{\sigma}}^o.\underline{\underline{Q}}\right)\right).\underline{\underline{Q}}^T = \dot{\underline{\underline{\sigma}}}^o + \underline{\underline{\sigma}}^o.\underline{\underline{\Omega}} - \underline{\underline{\Omega}}.\underline{\underline{\sigma}}^o \tag{29}$$

$\underline{\underline{Q}}$ is the rotation of the corotational (or spinless) frame which corresponds to the material spin:

$$\underline{\underline{\Omega}} = \frac{1}{2}\left(\nabla\dot{\underline{u}} - \nabla\dot{\underline{u}}^T\right) = \dot{\underline{\underline{Q}}}.\underline{\underline{Q}}^T \tag{30}$$

At the end $t^{i+1}$ of the time step, the mid-rule integration scheme of Hughes and Winget [36] gives the stress at $t^{i+1}$ from the strain increment:

$$[\boldsymbol{\sigma}^{o\,n+1}]_{e_i^{n+1}} = [\boldsymbol{\sigma}^{o\,n}]_{e_i^n} + [\mathbf{C}^{o\,n+1/2}]_{e_i^{n+1/2}}[\Delta\boldsymbol{\varepsilon}]_{e_i^{n+1/2}} \tag{31}$$

The orthonormal frame $\underline{e}_i$ is the local frame rotated by $\underline{\underline{Q}}$.

$$\Delta\boldsymbol{\varepsilon} = \mathbf{D}^{n+1/2}\Delta t = \mathbf{B}(\dot{\mathbf{u}}_n^e)^{n+1/2}\Delta t \tag{32}$$

where $\mathbf{B}$ is the standard strain interpolation matrix of the 8 node hexahedral element.

From stress, the internal nodal loads $\mathbf{F}_{\text{int}}^o$ of Eq. (4) are obtained as assembly on the preform of the elementary nodal load vectors $\mathbf{F}_{\text{int}}^{oe}$ such as:

$$\mathbf{F}_{\text{int}}^{oe} = \int_{V^e}\mathbf{B}^T\boldsymbol{\sigma}^o\mathrm{d}V \tag{33}$$

A reduced integration (i.e. a single Gauss point at the centre of the hexahedral element) is used to compute this integral.

*3.2.2. Plasticity*

An advantage of splitting the strain energy into two parts (4) is to allow to consider an elastic behaviour for yarn tensions and an elasto-plastic behaviour for other rigidities. Actually, during the forming of the interlock fabric, yarns stretching are small and have an elastic behaviour. Forming simulation allows to check that yarn extensions do not exceed the tension fracture limit. For the other parts of mechanical behaviour, there are generally permanent strains especially for global transverse compression and shear of the preform. These permanent deformations are due to friction between fibres and mechanical behaviour can be modelled by elasto-plastic models.

The main benefit of the hypoelastic models such as presented in Section 3.2.1 is that they are suitable for extension to plasticity (28) can be extended to:

$$\underline{\underline{\boldsymbol{\sigma}}}^{o\nabla} = \underline{\underline{\mathbf{C}}}^o : \left(\underline{\underline{\mathbf{D}}} - \underline{\underline{\mathbf{D}}}^p\right) \text{ with } \underline{\underline{\mathbf{D}}}^p = \dot{\lambda}\frac{\partial f}{\partial\boldsymbol{\sigma}} \tag{34}$$

$\underline{\underline{\mathbf{D}}}^p$ is the plastic stain rate, $f$ is the yield function and $\dot{\lambda}$ the plastic multiplier. Efficient prediction-correction algorithms such as the so-called "radial return" method have been developed to compute Cauchy stress from strain increment [33,39,42]. Identification of yield function in the case of interlock fabrics will be presented in

a future work. In the examples presented below, the behaviour is assumed to be elastic and the final state under consideration in the simulation of the forming process corresponds to the end of the tool displacement.

## 4. Simulations of standard tests

### *4.1. Tension, pure shear and simple shear elementary tests*

Several elementary tests (Fig. 7) have been performed to validate our method for taking into account yarns tension contribution: elements in tension, simple shear and pure shear. Error between simulated and analytical solution has been calculated with imposed displacements (Fig. 7e) or loads (Fig. 7f) for different yarns orientation in the element: yarns in direction *x*, *y*, *z*, and combined. The theoretical solution has been established considering an elastic relation between Cauchy stress and Hencky strain. Then, it has been checked that all unstretched yarns remain with a tension equal to zero, especially for transverse yarns in tension tests and for pure shear test. The results (Fig. 7) are sufficiently accurate to validate both method and implementation of a finite element able to take into account tension contribution of a discrete weaving of yarns.

### *4.2. Bias test*

After those elementary tests, standard tests used for fabric reinforcement shear characterization have been simulated. The bias test is a traction test on a sample oriented at 45°. It is much used and analyzed for the determination of composite reinforcement mechanical behaviour [17,43–48]. At the beginning of the test, yarns make a 45° angle with the deformation direction. This kinematics implies seven areas with three different behaviours; two are unsheared, one is sheared and the four others are half sheared (Fig. 8a–b). In those kinds of loadings, parameters that give stiffness are Young modulus and Poisson ratio from the hypoelastic model. Numerical simulation of a 3D woven specimen gives a deformation very close from the real test, and simulated behaviour compared with the measured one shows a good accuracy of the hypoelastic model especially knowing that it represents second-order terms. This test allows to validate the shearing contribution of our model.

## 5. 3D interlock fabric forming simulations

### *5.1. Hemispherical deep drawing*

Deep drawing simulations for 3D interlock fabrics have been performed. Fibre orientations clearly drive deformation as shown in Fig. 9, for two different orientations of yarns. This test have been intensively studied in the case of thin fabric reinforcements [23,49]. The simulation gives after forming the position of each yarn in the preform (Fig. 9b). This is important for further resin flow simulation and finite element analysis of the final composite part.

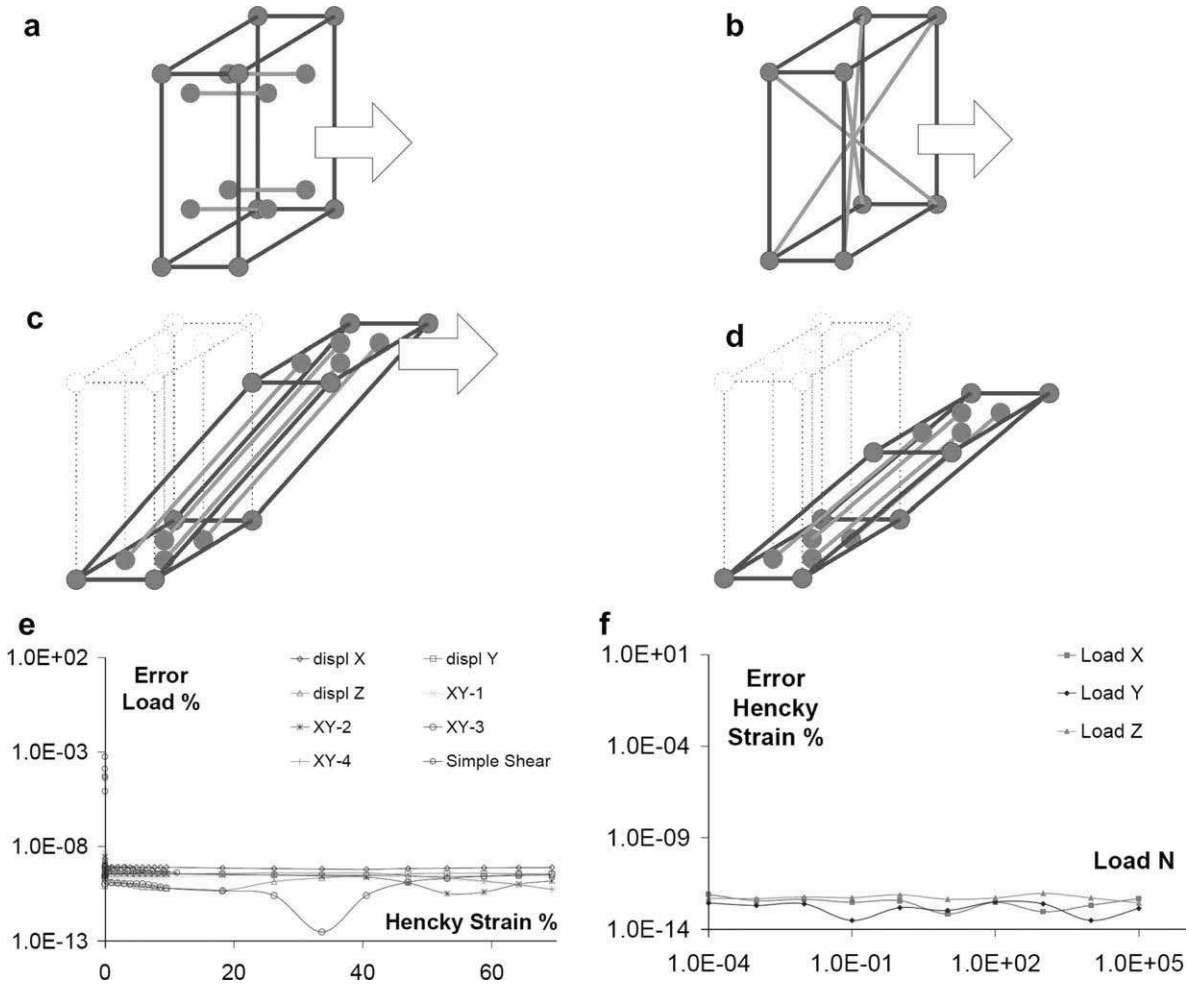


**Fig. 7.** Elementary tests (a) tension; (b) tension disoriented yarns; (c) simple shear; (d) pure shear; (e) error: imposed displacements and (f) error: imposed loads.

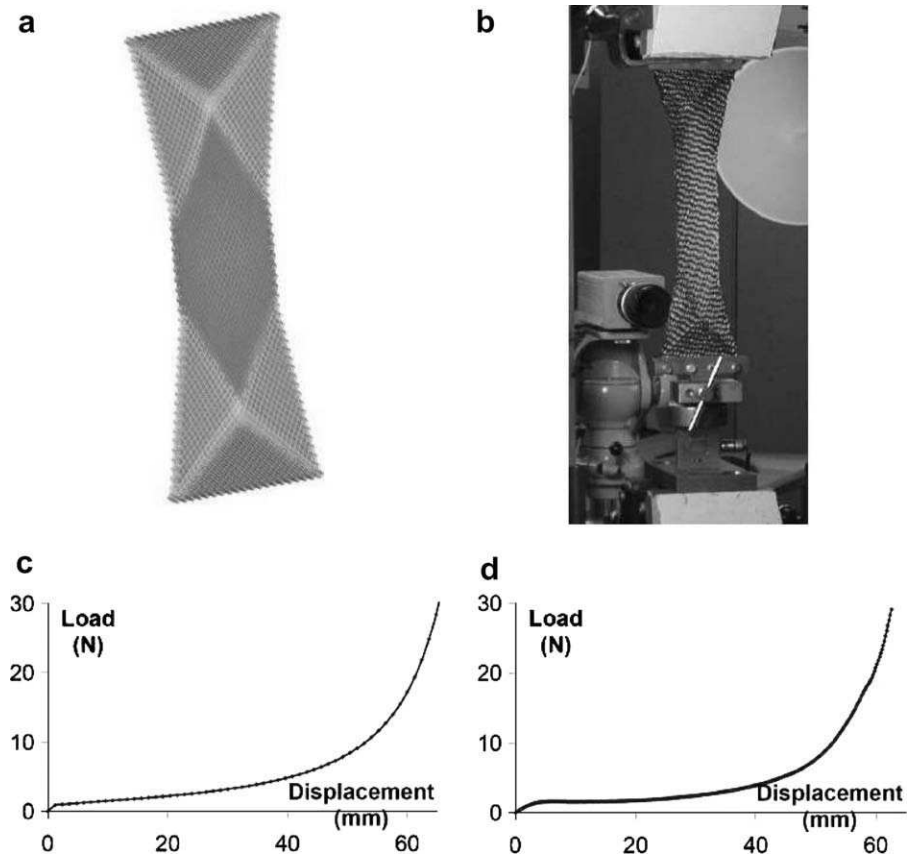


**Fig. 8.** Bias test (a) computed deformed shape; (b) bias test experiments; (c) computed load versus displacement and (d) measured load versus displacement.

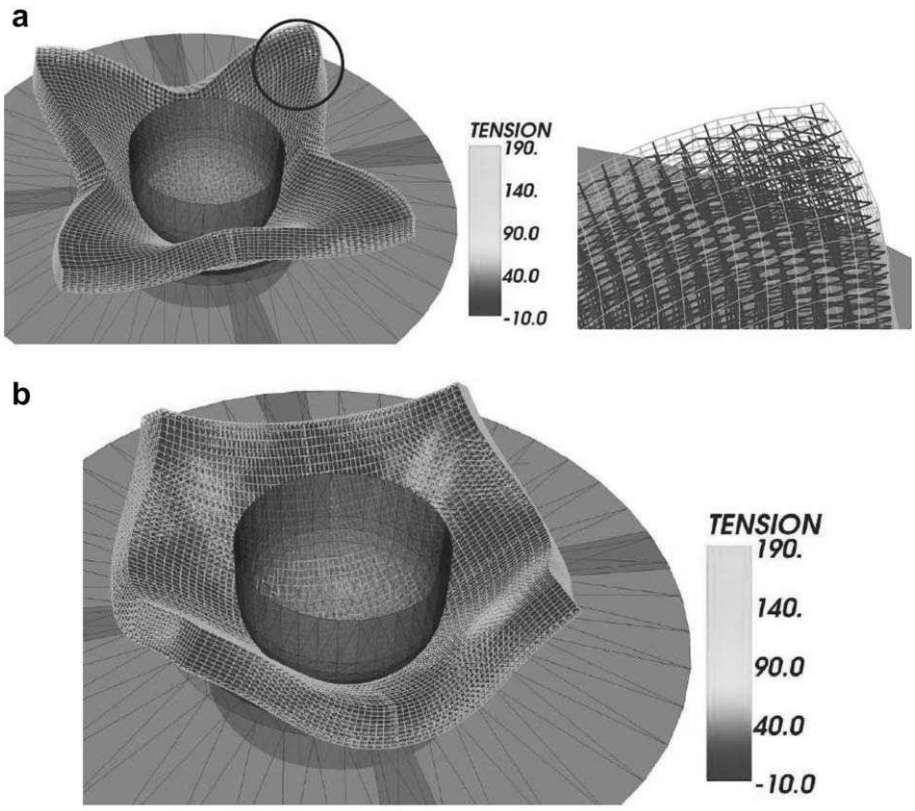


**Fig. 9.** Hemispherical deep drawing of a thick interlock preform (a) fibers orientation: +0° +90° and (b) fibers orientation: +45° −45°.

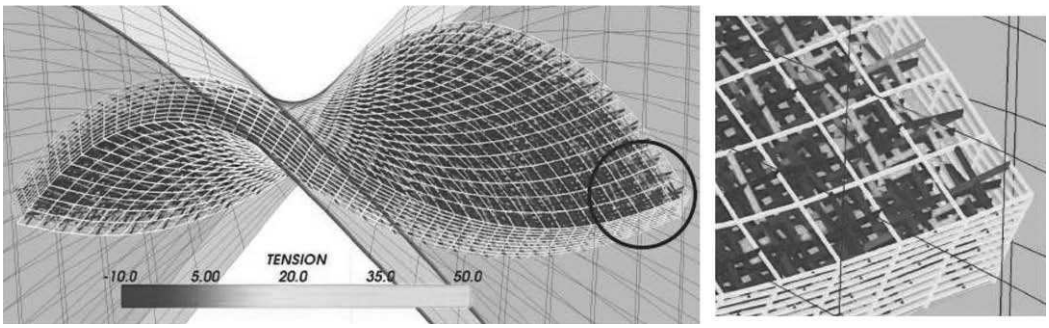


**Fig. 10.** Forming of a twisted plate.

*5.2. Forming of a twisted plate*

The objective of this model is to simulate forming of complex parts like motor blades with complex deformations, combination of shearing and twisting, and with varying thickness. A twisted plate forming simulation is performed as shown in Fig. 10. Comparisons with experimental 3D interlock forming are now in progress. The simulation gives the conditions for the feasibility of the forming process and above all, the position of fibers in the final part. These positions are essential for further structural computation.

## 6. Conclusions

A hexahedral finite element made of yarn segments has been proposed for the simulation of 3D interlock fabric forming. The position of each yarn within the finite element is taken into account. The rigidities due to transverse properties of the yarns are secondary. They are taken into account within a rate constitutive equation. These transverse phenomena are generally irreversible while the yarn tensile strains are elastic. The hypo-elasticity used to model the transverse properties can be conveniently extended to elasto-plasticity. The identification of the yield function in the case of interlock fabrics will be the next step of this work.

## Acknowledgement

The authors acknowledge the support provided by the SNECMA aeronautical company.

## References

[1] Pora J. Composite materials in the airbus A380 – from history to future. In: Proceedings of ICCM13, Plenary lecture, CD-ROM; 2001.
[2] Mazumdar S. Aerospace market forecast: what is in it for composites? High Performance Compos 2005. March.
[3] Beardman P. Automotive components: fabrication. In: Kelly A, editor. Concise encyclopedia of composite materials. Oxford: Pergamon Press; 1989. p. 24–31.
[4] Smith CS. Design of marine structures in composite materials. London: Elsevier Applied Science; 1990.
[5] Bowen DH. Applications of composites: an overview. In: Kelly A, editor. Concise encyclopedia of composite materials. Oxford: Pergamon Press; 1989. p. 7–15.
[6] Douthe C, Baverel O, Caron JF. Form-finding of a grid shell in composite materials. J Int Assoc Shell Spatial Struct 2006;47:53–62.
[7] Mouritz AP, Bannister MK, Falzon PJ, Leong KH. Review of applications for advanced three-dimensional fibre textile composites. Compos Part A 1999;30:1445–61.
[8] Tong L, Mouritz AP, Bannister MK. 3D Fibre reinforced polymer composites. Elsevier Science; 2002.
[9] Lomov SV, Gusakov A, Huysmans G, Prodromou AG, Verpoest I. Textile geometry preprocessor for meso-mechanical models of woven composites. Compos Sci Technol 2000;60(11):2083–95.
[10] Bigaud D, Dreano L, Hamelin P. Models of interactions between process, microstructure and mechanical properties of composite materials – a study of the interlock layer-to-layer braiding technique. Compos Struct 2005;67(1):99–114.
[11] Rudd CD, Long AC. Liquid Molding Technologies. ed. Woodhead Publishing Limited, 1997.
[12] Potter KD. History of the resin transfer moulding for aerospace applications. Compos Part A 1999;30:757–65.
[13] Parnas RS. Liquid composite molding. Hanser Garner publications; 2000.
[14] Van Der Ween F. Algorithms for draping fabrics on doubly curved surfaces. Int J Numer Method Eng 1991;31:1414–26.
[15] Hsiao S-W, Kikuchi N. Numerical analysis and optimal design of composite thermoforming process. Comput Methods Appl Mech Eng 1999;177:1–34.
[16] Dong L, Lekakou C, Bader MG. Processing of composites: simulations of the draping of fabrics with updated material behaviour law. J Compos Mater 2001;35(2):138–63.
[17] Peng X, Cao J. A continuum mechanics-based non-orthogonal constitutive model for woven composite fabrics. Compos Part A 2005;36:859–74.
[18] Boisse P, Zouari B, Daniel JL. Importance of in-plane shear rigidity in finite element analyses of woven fabric composite preforming. Compos Part A 2006;37(12):2201–12.
[19] Boisse P. Finite element analysis of composite forming. In: Long AC, editor. Composite forming technologies. Woodhead Publishing; 2007. p. 46–79. Chapter 3.
[20] Boisse P, Gasser A, Hagege B, Billoët JL. Analysis of the mechanical behaviour of woven fibrous material using virtual tests at the unit cell level. J Mater Sci 2005;40:5955–62.
[21] Ten Thije RHW, Akkerman R, Huetink J. Large deformation simulation of anisotropic material using an updated Lagrangian finite element method. Comput Methods Appl Mech Eng 2007;196(33-34):3141–50.
[22] Xue P, Cao J, Chen J. Integrated micro/macro-mechanical model of woven fabric composites under large deformation. Compos Struct 2005;70(1):69–80.
[23] Cherouat A, Billoët JL. Mechanical and numerical modelling of composite manufacturing processes deep-drawing and laying-up of thin pre-impregnated woven fabrics. J Mater Process Technol 2001;118:460–71.
[24] Sharma SB, Sutcliffe MPF. A simplified finite element model for draping of woven material. Compos Part A 2004;35:637–43.
[25] Ben Boubaker B, Haussy B, Ganghoffer JF. Discrete models of fabrics accounting for yarn interactions. Eur J Computat Mech 2005;14(6–7):653–76.
[26] Durville D. Numerical simulation of entangled materials mechanical properties. J Mater Sci 2005;40:5941–8.
[27] Pickett AK, Creech G, de Luca P. Simplified and advanced simulation methods for prediction of fabric draping. Eur J Computat Mech 2005;14(6-7):677–91.
[28] Duhovic M, Bhattacharyya D. Simulating the deformation mechanisms of knitted fabric composites. Compos Part A 2006;37(11):1897–915.
[29] Kawabata S, Niwa M, Kawai H. The finite-deformation theory of plain weave fabrics – part II: the uniaxial deformation theory. J Textile Inst 1973;64:47–61.
[30] Potluri P, Ariadurai S, Whyte IL. A general theory for deformation behaviour of non-plain weave fabrics under biaxial loading. J Textile Inst 2000;91-1(4):493–508.
[31] Belytschko T. An overview of semidiscretisation and time integration procedures. In: Belytschko T, Hughes TJR, editors. Computation methods for transient analysis. Elsevier Science; 1983. p. 1–65.
[32] Hughes TJH, Belytschko T. A precise of developments in computational methods for transient analysis. J Appl Mech 1983;50:1033–41.
[33] Criesfield MA. Non linear finite element analysis of solids and structure: advanced topics, vol. 2. Chichester: John Wiley and Sons; 1997.
[34] Zienkiewicz O, Taylor R. The finite element method, vol. 1. McGraw-Hill; 1989.
[35] Cox BN, Dadkhah MS, Morris WL. On the tensile failure of 3D woven composites. Compos Part A 1996;27(6):447–58.
[36] Hughes TJR, Winget J. Finite rotation effects in numerical integration of rate constitutive equations arising in large deformation analysis. Int J Numer Methods Eng 1980;15:1862–7.
[37] Bathe KJ. Finite element procedures. New JerseyEnglewood Cliffs, NJ: Prentice-Hall; 1996.
[38] Xiao H, Bruhns OT, Meyers A. Hypo-elasticity model based upon the logarithmic stress rate. J Elasticity 1997;47(1):51–68.
[39] Boubakar ML, Boisse P, Gelin JC. Numerical implementation of orthotropic plasticity for sheet metal forming analysis. J Mater Process Technol 1997;65:143–52.

[40] Belytschko T, Wing KL, Moran B. Nonlinear finite elements for continua and structures. Chichester: John Wiley and Sons; 2000.
[41] Dafalias YF. Corotational rates for kinematic hardening at large plastic deformations. Trans ASME J Appl Mech 1983;50:561–5.
[42] Ortiz M, Simo JC. An analysis of a new class of integration algorithms for elastoplastic constitutive relations. Int J Numer Methods Eng 1986;23:353–66.
[43] Prodromou AG, Chen J. On the relationship between shear angle and wrinkling of textile composite preforms. Compos Part A 1997;28(5):491–503.
[44] Potter K. Bias extension measurements on cross-plied unidirectional prepreg. Compos Part A 2002;33(1):63–73.
[45] Lebrun G, Bureau MN, Denault J. Evaluation of bias-extension and picture-frame test methods for the measurement of intraply shear properties of PP/glass commingled fabrics. Compos Struct 2003;61(4):341–52.
[46] Lomov SV, Willems A, Barburski M, Stoilova TZ, Verpoest I, Zhu Y. Picture frame test of woven composite reinforcements with a full-field strain registration. Textile Res J 2006;76:243–52.
[47] Potluri P, Perez Ciurezu D, Ramgulam R. Measurement of meso-scale shear deformations for modelling textile composites. In: CompTest 2004, Compos Part A 2006;37(2):303–314.
[48] Lomov SV, Boisse P, Deluycker E, Morestin F, Vanclooster K, Vandepitte D, et al. Full-field strain measurements in textile deformability studies. Compos Part A 2007. doi:10.1016/j.compositesa.2007.09.014.
[49] Lin H, Wang J, Long AC, Clifford MJ, Harrison P. Predictive modelling for optimization of textile composite forming. Compos Sci Technol 2007;67(15-16):3242–52.